

# G<sup>2</sup>VD Planner: An Efficient Motion Planning Approach With Grid-based Generalized Voronoi Diagrams

Jian Wen, Xuebo Zhang<sup>†</sup>, Hui Liu, Haoyue Liu, Jing Yuan, and Yongchun Fang

**Abstract**—In this letter, an efficient motion planning approach with grid-based generalized Voronoi diagrams (G<sup>2</sup>VD) is newly proposed for mobile robots. Different from existing approaches, the novelty of this work is twofold: 1) a new state lattice-based path searching approach is proposed, in which the search space is reduced to a Voronoi corridor to further improve the search efficiency, along with a Voronoi potential field constructed to make the searched path keep a reasonable distance from obstacles to provide sufficient optimization margin for the subsequent path smoothing, and 2) an efficient quadratic programming-based path smoothing approach is presented, wherein the clearance to obstacles is considered in the form of the penalty of the deviation from the safe reference path to improve the path clearance of hard-constrained path smoothing approaches. We validate the efficiency and smoothness of our approach in various challenging simulation scenarios and large-scale outdoor environments. It is shown that the computational efficiency is improved by 17.1% in the path searching stage, and smoothing the path with our approach is 11.86 times faster than a recent gradient-based path smoothing approach. We will release the source code to the robotics community<sup>1</sup>.

## I. INTRODUCTION

Mobile robots have been widely applied in various fields including but not limited to family service, logistics, and search-and-rescue applications. Motion planning is one of the key technologies for mobile robots to achieve full autonomy in these scenarios and plays an essential role in generating safe, smooth, and efficient motions [1]–[3].

### A. Path Searching

Sampling-based planning and grid-based planning are two popular path searching approaches. Sampling-based planning algorithms such as the famous probabilistic roadmap (PRM) [4] and rapidly-exploring random tree (RRT) [5] have gained the popularity for the capability of efficiently searching in the configuration space (C-space). However, they are limited by completeness and optimality, and even some excellent variants such as RRT\* [6] can only guarantee asymptotic optimality. In this letter, we focus on grid-based planning. Grid-based planning overlays a hyper-grid on the C-space and assumes each configuration is identified with the grid-cell center. Then, search algorithms such as A\* [7] are used to find a path from the start to the goal. Grid-based planning

The authors are with the Institute of Robotics and Automatic Information System, College of Artificial Intelligence, Nankai University, Tianjin 300350, China, and also with the Tianjin Key Laboratory of Intelligent Robotics, Nankai University, Tianjin 300350, China (e-mail: zhangxuebo@nankai.edu.cn; wenjian@mail.nankai.edu.cn).

<sup>†</sup>: Corresponding author.

<sup>1</sup>The open-source code will be released at our website [https://github.com/NKU-MobFly-Robotics/g2vd\\_planner](https://github.com/NKU-MobFly-Robotics/g2vd_planner).

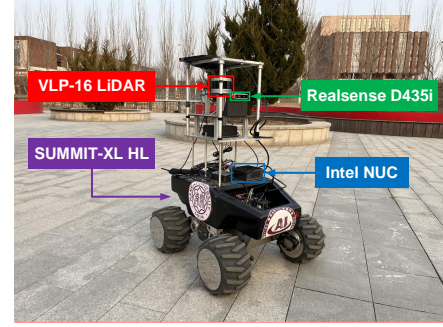


Fig. 1. Our experimental mobile robot SUMMIT-XL HL is equipped with a Velodyne VLP-16 LiDAR, an Intel Realsense D435i depth camera, and an Intel NUC computer. Experiments are detailed in Section VI and the video is available at [https://youtu.be/V-S8cS2zv\\_U](https://youtu.be/V-S8cS2zv_U).

can always find a resolution-optimal path if it exists in the discrete search space. However, these approaches depend on the space discretization and do not perform well as the environment dimension increases. In addition, most path searching algorithms only consider the path length in the cost function, which often results in the searched path being close to obstacles and poor safety.

### B. Path Smoothing

The path obtained by path searching approaches usually fails to meet the smoothness requirement for robot navigation and needs further smoothing [8]. Two types of path smoothing approaches are investigated in this letter, namely, soft-constrained approaches and hard-constrained approaches.

1) *Soft-constrained Approaches*: These approaches formulate path smoothing as a non-linear unconstrained optimization problem, wherein the constraints are considered in the optimization objective in the form of penalty cost terms. Generally, the smoothness of the path and the clearance to obstacles are both taken into account. Then, gradient-based optimization algorithms are employed to solve the problem. Soft-constrained approaches utilize gradient information to push the path far from obstacles and can obtain a smooth path with a reasonable distance from obstacles. However, it is difficult for these approaches to guarantee the optimized path strictly satisfies the constraints. In addition, the optimization objective of soft-constrained approaches contains convex and non-convex terms, making these approaches suffer from local optima and time-consuming.

2) *Hard-constrained Approaches*: These approaches formulate path smoothing as a non-linear constrained optimization problem and can obtain a path that theoretically satisfies

the constraints. The optimization objective usually considers the smoothness or the length of the path and thus is convex. This convexity allows the problem to be solved efficiently. However, hard-constrained approaches treat all free space equally, namely, distance from the free space to obstacles is ignored. As a result, the optimized path may be close to obstacles and is dangerous for robot navigation.

### C. Contributions

Motivated by the aforementioned limitations of existing approaches, an efficient motion planning approach called  $G^2VD$  planner is newly proposed for mobile robots. Specifically, a grid-based generalized Voronoi diagram ( $G^2VD$ ) is utilized to aid path searching and path smoothing to achieve better performance.

1) *Path Searching*: Given the start and the goal, we first employ the  $A^*$  search to find the shortest grid path in a grid-based GVD. This shortest Voronoi path contains the topological information of the search direction and provides rough guidance for the subsequent fine search. Along the Voronoi grid path, a region called *Voronoi corridor* is constructed by adding a bounding box to each path pixel. Furthermore, the cost function of path searching is redesigned based on a potential called *Voronoi field* to make the searched path keep a reasonable distance from obstacles. Finally, the  $A^*$  search combined with motion primitives is utilized to finely search a kinematically feasible path within the Voronoi corridor. Different from the original state lattice-based path planner [9] that takes the whole grid map as the search space, the proposed approach reduces the search space to the Voronoi corridor, thus considerable time is saved for path searching. In addition, the reasonable clearance to obstacles provides sufficient optimization margin for further path smoothing.

2) *Path Smoothing*: Taking the path searched above as the reference path, an efficient quadratic programming (QP)-based path smoothing approach is proposed, wherein the smoothness of the path and the deviation from the reference path are considered in the optimization objective. Our goal is to obtain a smooth path while minimizing the deviation between the optimized path and the reference path. Because the reference path searched above has a certain distance to obstacles, the clearance to obstacles is indirectly considered in the proposed approach, and the final smoothed path will not be close to obstacles, which is usually difficult for hard-constrained approaches. This is also the second reason that we introduce the Voronoi field to improve the path clearance of the searched path, in addition to providing wider optimization margin for path smoothing.

To summarize, the main contributions of this letter are as follows:

- 1) A new state lattice-based path planner is proposed, in which the search space is reduced to a Voronoi corridor to improve the search efficiency, along with a Voronoi potential constructed to make the searched path keep a reasonable distance from obstacles to provide sufficient optimization margin for further path smoothing.

- 2) An efficient QP-based path smoothing approach is presented, wherein the clearance to obstacles is considered in the form of the penalty of the deviation from the safe reference path to improve the path clearance of hard-constrained path smoothing approaches.
- 3) Autonomous navigation is realized in large-scale outdoor environments. Extensive simulation and experimental evaluations are presented to validate the effectiveness of the proposed approach. We will release the source code to the robotics community.

The rest of this letter is organized as follows. We first review the related work in Section II. The proposed  $G^2VD$  planner is detailed in Section III. Section IV provides some implementation details. The results of simulations and experiments are presented in Sections V and VI, respectively. Finally, this letter is concluded in Section VII.

## II. RELATED WORK

Grid-based planning obtains the resolution-optimal path by discretizing the C-space first and then using graph search algorithms to find the path. However, original grid-based planning approaches only visit the centers of grid cells and produce piecewise-linear paths that do not generally satisfy the kinodynamic constraints of the robot. To address this problem, Pivtoraiko *et al.* [10] propose the state lattice approach for graph construction. In particular, the connectivity between two nodes in the graph is built from a pre-designed motion primitive that fulfills the kinodynamic constraints of the robot. Based on the work [10], Likhachev *et al.* present the state lattice-based path planner by combining  $AD^*$  search with motion primitives [9], which has been successfully applied in the DARPA Urban Challenge [11]. In this letter, a new state lattice-based path planner is proposed, wherein the search space is reduced to a Voronoi corridor derived based on a generalized Voronoi diagram (GVD) to further improve the search efficiency.

The use of GVDs has long been proposed in the context of robot motion planning. In [12], Choset and Burdick use the GVD to derive skeletons of the free space and then search on the graph. However, the shortest Voronoi path may be far from the actual optimal path. In [13], Ziegler *et al.* utilize the GVD to inform the  $A^*$  search by constructing a heuristic where the cost of a search state is the sum of the straight-line path to the closest Voronoi edge and the shortest path along the GVD edges. However, the resulting heuristic cannot be guaranteed to be admissible since the cost of the shortest Voronoi path may be greater than that of the actual shortest path. In [14], Dolgov *et al.* present a potential field based on the GVD for path smoothing. This potential allows precise navigation in narrow passages while also effectively pushing the robot away from obstacles in wider areas. Inspired by the Voronoi field, we redesign the cost function of the state lattice-based path planner to obtain a path with a reasonable distance from obstacles.

The path obtained by path searching approaches usually needs further smoothing. In [14], Dolgov *et al.* present a conjugate gradient (CG)-based path smoothing approach to

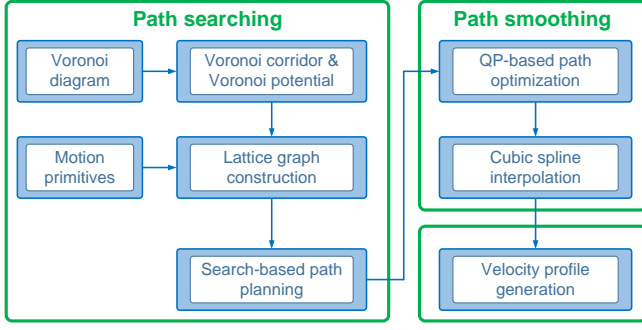


Fig. 2. Flow chart of the proposed three-layer motion planning framework.

smooth the path generated by the hybrid A\* algorithm. In [15], Wen *et al.* propose a gradient-based local path smoothing approach for mobile robots, wherein the sparse-banded system structure of the underlying optimization problem is fully exploited to efficiently solve the problem. The above soft-constrained approaches utilize gradient information to push the path far from obstacles and can obtain a path with better safety. However, it is difficult for these approaches to guarantee the optimized path strictly satisfies the constraints. Recently, Zhou *et al.* propose a dual-loop iterative anchoring path smoothing (DL-IAPS) approach for autonomous driving [16], in which the nonlinear curvature constraint is linearized and sequential convex programming (SCP) is used to efficiently solve the path optimization problem. Such a hard-constrained approach can theoretically guarantee that the obtained path strictly satisfies the constraints. However, distance from the free space to obstacles is ignored, which often results in the optimized path being close to obstacles and poor safety. In this letter, a new QP-based path smoothing approach is proposed, in which the clearance to obstacles is indirectly considered in the form of the penalty of the deviation from the safe reference path to improve the path clearance of hard-constrained approaches.

### III. G<sup>2</sup>VD PLANNER

In this letter, a three-layer motion planning framework called G<sup>2</sup>VD planner is carefully designed, which consists of path searching, path smoothing, and velocity planning, as shown in Fig. 2. The path searching module is utilized to provide a safe reference path for the robot, and the path smoothing module combined with our previously proposed time-optimal velocity planning [17] is employed to generate safe, smooth, and efficient motion commands. In this section, we will detail the newly proposed path searching and path smoothing modules.

#### A. Grid-based Generalized Voronoi Diagrams

The GVD is defined as the set of points in the free space to which the two closest obstacles have the same distance [12]. In this letter, an efficient, incrementally updatable GVD construction algorithm presented in [18] is utilized to convert the occupancy grid map to a GVD in discrete form. This algorithm [18] employs a wavefront algorithm to perform distance transforms. Therefore, every cell in the grid-based

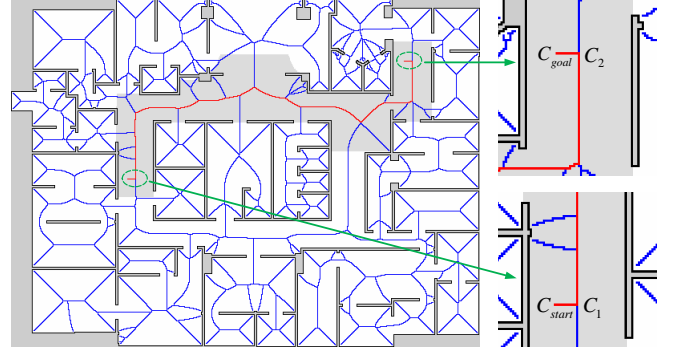


Fig. 3. Grid-based GVD of an office-like environment. The GVD edge pixels are colored in blue and red, and the searched shortest Voronoi path is colored in red. The gray region surrounding the Voronoi path denotes the Voronoi corridor.

GVD stores not only the state of whether it belongs to the GVD but also the minimum Euclidean distance to the closest obstacle cell. Fig. 3 illustrates the grid-based GVD of an office-like environment, in which the GVD edge pixels are colored in blue and red.

#### B. Voronoi Corridor

After obtaining the grid-based GVD, breadth-first search is employed to find the cells  $C_1$  and  $C_2$  closest to the start cell  $C_{start}$  and the goal cell  $C_{goal}$  on the GVD, respectively. And the shortest grid paths  $L_1$  from  $C_{start}$  to  $C_1$  and  $L_2$  from  $C_2$  to  $C_{goal}$  are also computed in this process. Then, the A\* search is utilized to search the shortest grid path  $L_3$  from  $C_1$  to  $C_2$  along the GVD edge pixels. The final shortest Voronoi path from  $C_{start}$  to  $C_{goal}$  is composed of  $L_1$ ,  $L_3$ , and  $L_2$ , as shown by the red path in Fig. 3.

Based on the shortest Voronoi grid path searched above, a region called Voronoi corridor is constructed as follows. For every cell  $C_k$  in the shortest Voronoi grid path, the minimum distance to the closest obstacle cell  $d_k$  is retrieved from the grid-based GVD. Then, a square bounding box with a side length of  $2d_k$  is centered on  $C_k$ . The obstacle-free cells covered by all bounding boxes make up the Voronoi corridor, as illustrated by the gray region in Fig. 3.

#### C. Path Searching

The shortest Voronoi path is far from the actual optimal path, and its piecewise-linear form also does not satisfy the kinodynamic constraints of the robot. To address these issues, a new state lattice-based path planner is proposed to perform fine path searching within the Voronoi corridor.

A typical state lattice-based path planner consists of two parts, namely, graph construction and graph search [9]. As for graph construction, the 3-D search space  $(x, y, \theta)$  is discretized first, where  $(x, y)$  denotes the position of the robot in the world and  $\theta$  represents the heading of the robot. In particular, the orientation space is discretized into 16 angles. Furthermore, the connectivity between two states in the graph is built from motion primitives which fulfill the kinematic constraints of the robot. In this letter, a quintic Bézier curve-based path generation approach described in

[19] is employed to generate motion primitives offline. A motion primitive  $\gamma(s, s')$  consists of a sequence of internal robot poses when moving from state  $s$  to state  $s'$ . As for graph search, the standard A\* search is employed, where the 2-D heuristic  $h_{2D}$  proposed in [9] is utilized to guide the A\* search away from those areas with dead-ends. This heuristic is constructed by computing the costs of shortest 2-D grid paths from the goal cell to other cells in the search space through Dijkstra's algorithm. Different from the original state lattice-based path planner [9] that takes the whole grid map as the search space, we reduce the search space to the Voronoi corridor to further improve the search efficiency. In addition, every time the grid map is updated,  $h_{2D}$  needs recalculation before performing path searching. Since the search space of the newly proposed state lattice-based path planner is reduced to the Voronoi corridor, Dijkstra's search is accordingly restricted to only compute the costs of shortest paths from the goal cell to those cells that are within the Voronoi corridor. Therefore, considerable time is also saved for the recalculation of  $h_{2D}$ .

Although the path searched above is optimal in the search space, it may be very close to obstacles. The ideal path is to keep a reasonable distance from obstacles to provide sufficient optimization margin for subsequent path smoothing. To this end, inspired by the Voronoi field presented in [14], we design the following potential function:

$$\rho_V(x, y) = \begin{cases} \frac{d_V(x, y)}{d_O(x, y) + d_V(x, y)} \frac{(d_O - d_O^{\min})^2}{(d_O^{\min})^2} & d_O \leq d_O^{\min} \\ 0 & d_O > d_O^{\min} \end{cases} \quad (1)$$

where  $d_V(x, y)$  and  $d_O(x, y)$  denote the distances from the given path vertex  $(x, y)$  to the closest Voronoi edge and the closest obstacle, respectively.  $d_O^{\min}$  is a threshold specifying the minimum safety distance to obstacles.

According to [14], this potential function has the following properties:

- i)  $\rho_V(x, y) \in [0, 1]$  and is continuous on  $(x, y)$  since we cannot simultaneously have  $d_V = 0$  and  $d_O = 0$ ;
- ii)  $\rho_V(x, y)$  reaches its maximum only when  $(x, y)$  is within obstacle areas;
- iii)  $\rho_V(x, y)$  reaches its minimum only when  $(x, y)$  is on the edges of the GVD or the distance from  $(x, y)$  to the closest obstacle is greater than  $d_O^{\min}$ .

It is noteworthy that the potential cost is set to zero when the distance to the closest obstacle is greater than the safety threshold ( $d_O > d_O^{\min}$ ). The reason for this design is as follows. Our goal is to make the searched path close to Voronoi edges through the Voronoi field so that the obtained path can keep an appropriate distance from obstacles and provide sufficient optimization margin for subsequent path smoothing. However, if the environment is wider and the Voronoi edge is far from the obstacles on both sides, which may make the searched path far away from the optimal path. Therefore, we set a safety distance threshold  $d_O^{\min}$  and regard

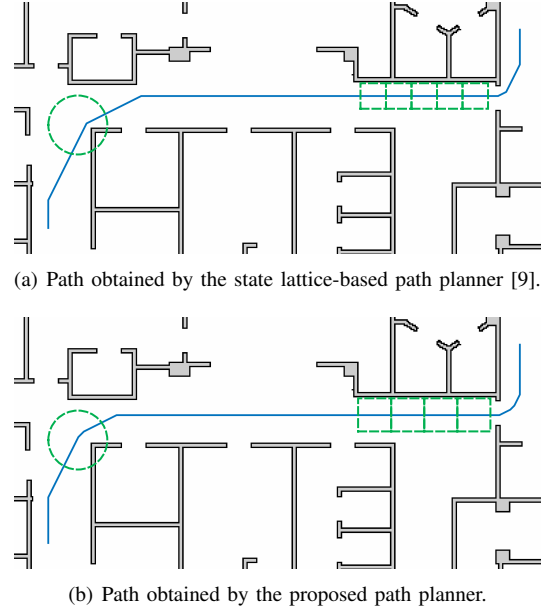


Fig. 4. Illustration of path searching results.

the area where the distance to the closest obstacle exceeds  $d_O^{\min}$  as a safe region. In this way, the searched path can keep a certain distance from obstacles and will not be far away from the optimal path through the Voronoi field.

Based on the above Voronoi field, the cost of motion primitives is defined as follows. For the sake of computational efficiency, we broadly follow the work [14] and temporarily assume that the robot travels at constant linear and angular velocities. If a motion primitive  $\gamma(s, s')$  collides with obstacles, the cost  $g(\gamma(s, s'))$  is set to infinity. Otherwise, the cost of this motion primitive is defined as

$$g(\gamma(s, s')) = t(s, s') \cdot \left( \max_{(x, y) \in Q} \rho_V(x, y) + 1 \right), \quad (2)$$

where  $t(s, s')$  is the travel time spent on  $\gamma(s, s')$  assuming uniform motion,  $Q$  is the set of 2-D cells covered by the robot when moving from state  $s$  to state  $s'$ . Intuitively, the Voronoi field penalizes slightly more those actions for which the robot traverses high potential cost areas (e.g., obstacles) and makes the searched path as close as possible to the Voronoi edges or keep a certain distance from obstacles. In addition, the 2-D heuristic  $h_{2D}$  is also multiplied by the potential costs to be consistent with the cost definition of motion primitives.

It should be noted that the Voronoi potential field in [14] is used for path smoothing and the region of interest is the whole map. While the search space of the newly proposed state lattice-based path planner is reduced to the Voronoi corridor, and we only need to compute the Voronoi potential costs within the Voronoi corridor. In particular, an efficient distance transform algorithm presented in [20] is employed to compute the Euclidean distance to the closest Voronoi edge for those cells within the Voronoi corridor. Figs. 4(a) and 4(b) illustrate the paths searched by the original state lattice-based path planner [9] and the newly proposed path planner, respectively. Compared with the original state lattice-based



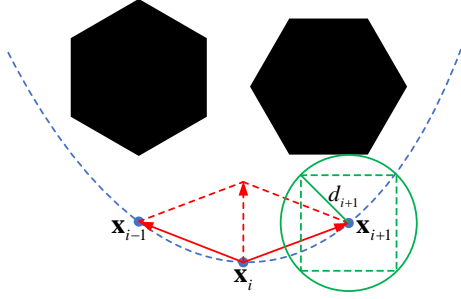


Fig. 5. Illustration of path smoothing formulation.  $\mathbf{x}_{i-1}$ ,  $\mathbf{x}_i$ , and  $\mathbf{x}_{i+1}$  denote three successive path vertices.  $d_{i+1}$  is the distance from  $\mathbf{x}_{i+1}$  to the closest obstacle. The black blocks represent obstacles.

path planner, the path obtained by the proposed path planner has a certain distance from obstacles and can provide wider optimization margin (green bounding boxes) for further path smoothing, which will be detailed in Section III-D.

#### D. Path Smoothing

The path obtained by the state lattice-based path planner is kinematically feasible, but it is still piecewise-linear and not suitable for velocity planning. Therefore, an efficient QP-based path smoothing approach combined with cubic spline interpolation is employed to further smooth the path.

The input of path smoothing is several reference path vertices obtained by sampling in the path generated by the state lattice-based path planner with a fixed interval. In consideration of the smoothness of the path and the deviation from the reference path, a convex QP-based path smoothing formulation is defined as

$$\min_{\mathbf{x}} \omega_s \sum_{i=2}^{n-1} \|\mathbf{x}_{i+1} - 2\mathbf{x}_i + \mathbf{x}_{i-1}\|^2 + \omega_r \sum_{i=1}^n \|\mathbf{x}_i - \mathbf{x}_{i_{ref}}\|^2, \quad (3)$$

subject to:

$$\mathbf{x}_1 = \mathbf{x}_{1_{ref}} \text{ and } \mathbf{x}_n = \mathbf{x}_{n_{ref}}, \quad (4a)$$

$$\mathbf{x}_i \in \mathcal{B}_i, \text{ for } i = 2, \dots, n-1. \quad (4b)$$

Here,  $\mathbf{x} = [\mathbf{x}_1^T \mathbf{x}_2^T \dots \mathbf{x}_n^T]^T$  is a  $2n$ -dimensional parameter vector, where  $\mathbf{x}_i = (x_i, y_i)^T$ ,  $1 \leq i \leq n$  denotes the world coordinates of a path vertex.  $\mathbf{x}_{i_{ref}} = (x_{i_{ref}}, y_{i_{ref}})^T$ ,  $1 \leq i \leq n$  is the corresponding reference path vertex of  $\mathbf{x}_i$ , and  $\omega_s$  and  $\omega_r$  are the weights of cost terms.  $\mathcal{B}_i$  is a state bubble constraining the feasible region of the path vertex  $\mathbf{x}_i$ . In this letter,  $\mathcal{B}_i$  is approximated as an inscribed square of a circle centered on  $\mathbf{x}_{i_{ref}}$  with the radius of the distance  $d_i$  from  $\mathbf{x}_{i_{ref}}$  to the closest obstacle, as shown in Fig. 5. Taking the circumscribed radius  $r_c$  of the robot into account, Eq. (4b) is approximated as:

$$x_{i_{ref}} - b_i \leq x_i \leq x_{i_{ref}} + b_i, \quad (5a)$$

$$y_{i_{ref}} - b_i \leq y_i \leq y_{i_{ref}} + b_i, \quad (5b)$$

where

$$b_i = \begin{cases} \frac{\sqrt{2}}{2}d_i - r_c & \frac{\sqrt{2}}{2}d_i > r_c \\ 0 & \frac{\sqrt{2}}{2}d_i \leq r_c. \end{cases} \quad (6)$$

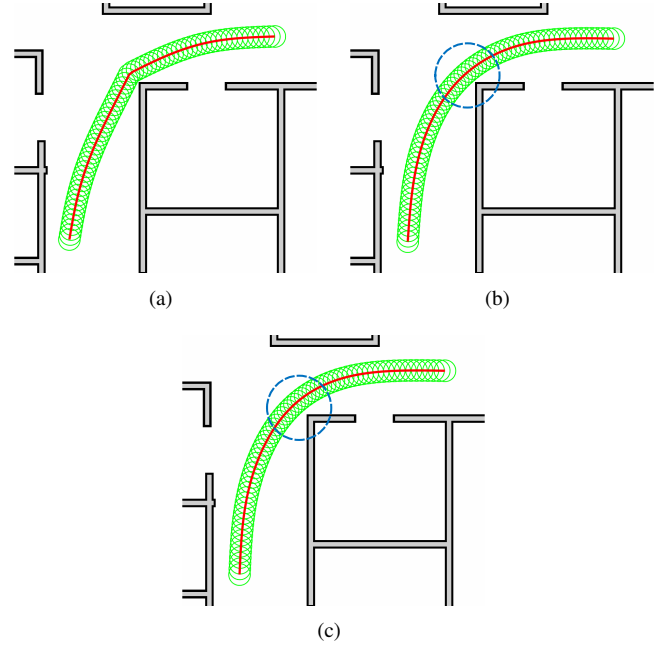


Fig. 6. Illustration of path smoothing results. Green circles denote the circumscribed radius of the robot. (a) Smoothed path with the path shown in Fig. 4(a) as input. (b) Smoothed path with the path shown in Fig. 4(b) as input but without penalizing the deviation from the reference path. (c) Smoothed path with the path shown in Fig. 4(b) as input and penalizing the deviation from the safe reference path.

The first term in Eq. (3) is a measure of the path smoothness. The cost function  $\mathbf{x}_{i+1} - 2\mathbf{x}_i + \mathbf{x}_{i-1}$  can be rewritten as  $(\mathbf{x}_{i+1} - \mathbf{x}_i) + (\mathbf{x}_{i-1} - \mathbf{x}_i)$ . As shown in Fig. 5, from a physical point of view, this cost term treats the path as a series spring system, where  $\mathbf{x}_{i+1} - \mathbf{x}_i$  and  $\mathbf{x}_{i-1} - \mathbf{x}_i$  are the forces on the two springs connecting the vertices  $\mathbf{x}_{i+1}$ ,  $\mathbf{x}_i$  and  $\mathbf{x}_{i-1}$ ,  $\mathbf{x}_i$ , respectively. If the forces  $\mathbf{x}_{i+1} - \mathbf{x}_i$  and  $\mathbf{x}_{i-1} - \mathbf{x}_i$  are equal in size and opposite in direction, the resultant force  $(\mathbf{x}_{i+1} - \mathbf{x}_i) + (\mathbf{x}_{i-1} - \mathbf{x}_i)$  is a zero vector and the norm is minimum. If all the resultant forces are zero vectors, all the vertices would uniformly distribute in a straight line, and the path is ideally smooth.

The second term in Eq. (3) is used to penalize the deviation from the original safe reference path. As mentioned before, the hard-constrained formulation does not explicitly consider the path clearance, namely, distance from the free space to obstacles is ignored. As a result, the optimized path may be close to obstacles. To address this issue, the penalty of the deviation from the original reference path is introduced in the optimization objective. Our goal is to obtain a smooth path while minimizing the deviation between the optimized path and the reference path. Because the reference path searched by the proposed state lattice-based path planner has certain clearance to obstacles, the safety of the path is indirectly considered in the optimization formulation, and the final optimized path will not be close to obstacles. This is also the second reason that we introduce the Voronoi field to make the searched path keep a reasonable distance from obstacles in Section III-C, in addition to providing wider optimization margin for path smoothing as mentioned before.

After path optimization, a path that is much smoother than the original reference path is obtained. However, the number of the path vertices is the same as that of the input reference path and the path is still piecewise-linear. Therefore, we further smooth the path via cubic spline interpolation to get a continuous curve.

Fig. 6(a) depicts the smoothed path with the path generated by the original state lattice-based path planner (as shown in Fig. 4(a)) as input. Since the path obtained by the original state lattice-based path planner is close to obstacles, the path vertices near the corner are fixed during path optimization, and the final smoothed path is intuitively rough. On the contrary, the path generated by the proposed path planner (as shown in Fig. 4(b)) keeps a certain distance from obstacles and provides sufficient optimization margin for path smoothing. As a result, the smoothed paths illustrated in Figs. 6(b) and 6(c) are much smoother than the path shown in Fig. 6(a). Compared with the path shown in Fig. 6(b), the deviation from the safe reference path is considered in Fig. 6(c), thus the path clearance of the final smoothed path is improved.

#### IV. IMPLEMENTATION DETAILS

##### A. Setup

G<sup>2</sup>VD planner is implemented in C/C++. The convex QP problem described in Section III-D is solved by an alternating direction method of multipliers (ADMM)-based QP solver, OSQP [21]. The reference path of path smoothing is obtained by sampling in the path generated by the state lattice-based path planner with an interval of 0.1 m. In consideration of the computational efficiency and sensing range, the cumulative length of the reference path is set to 4.0 m. The weights  $\omega_s$  and  $\omega_r$  are empirically set to 10 and 1, respectively. In the future, we plan to use machine learning techniques to tune these weights adaptively.

##### B. Metrics

The proposed Voronoi corridor is integrated into the original state lattice-based path planner (A\* + motion primitives) [9] to derive a new state lattice-based path planner (A\* + motion primitives + Voronoi corridor). And the new path planner is compared with the original state lattice-based path planner to validate the effectiveness of the Voronoi corridor. The performance of path searching approaches is evaluated in terms of *computational efficiency* and *memory consumption*. In particular, the number of expanded states and the planning time are used to evaluate the computational efficiency, and the graph size, i.e., the number of created nodes in the search graph, is used to evaluate the memory consumption.

To validate the effectiveness of the proposed QP-based path smoothing approach, we compare it with a recent gradient-based path smoothing approach SBA [15]. We comprehensively evaluate path smoothing approaches in terms of *travel distance*, *efficiency*, and *smoothness*. In particular, the time  $T$  taken by the robot to complete the navigation task is employed to evaluate the motion efficiency, the computational efficiency  $C$  is measured as the time consumption of a single path optimization, and the smoothness is evaluated by

TABLE I  
QUANTITATIVE STATISTICS OF PATH PLANNING RESULTS IN SIMULATION

		# of expands	Time (secs)	Graph size	Path cost
Test 1	Lattice	155,715	0.115	161,848	291,590
	Ours	<b>140,909</b>	<b>0.097</b>	<b>144,943</b>	291,590
Test 2	Lattice	167,912	0.122	174,356	324,846
	Ours	<b>146,300</b>	<b>0.103</b>	<b>149,912</b>	324,846
Test 3	Lattice	202,680	0.151	210,043	383,376
	Ours	<b>169,949</b>	<b>0.121</b>	<b>173,716</b>	383,376

the maximum curvature  $K_{max}$  and mean curvature  $K_{mean}$ . The curvature is calculated by computing the turning radius of the robot based on the assumption that path vertices are uniformly and densely spread over the path [16]. To satisfy this condition, cubic spline interpolation is utilized to smooth the traveling route of the robot to get a continuous curve. Then, we densely sample path vertices on the curve to compute the curvature.

#### V. SIMULATIONS

In this section, we verify the applicability of the proposed G<sup>2</sup>VD planner in simulation based on the popular Gazebo simulator [22]. The simulation scenarios designed in [23] are used for evaluation<sup>2</sup>.

##### A. Comparison on Path Searching

We choose the large-scale complex maze scenario in [23] to evaluate the performance of path searching approaches. Furthermore, we randomly select three sets of start and goal configurations in the maze for testing. Both the original state lattice-based path planner and the proposed path planner generate equal quality paths. Table I enumerates some quantitative statistics of path searching results in these tests.

Since the search space is reduced to the Voronoi corridor, the search direction is focused towards the most promising search areas, and the computational efficiency of graph search is improved. Compared with the original state lattice-based path planner, the number of the expanded search states of the proposed path planner decreases by an average of 12.8%, and the computational efficiency is improved by 17.1%. Furthermore, since the search branches for searching in those unpromising search areas are reduced, the number of created nodes in the search graph decreases. Compared with the original state lattice-based path planner, the graph size of the proposed path planner decreases by an average of 13.9%. In conclusion, the newly proposed path planner generates equal quality paths with less time and memory consumption than the original state lattice-based path planner.

##### B. Comparison on Path Smoothing

We choose three challenging scenarios of large-scale shopping mall, complex maze, and narrow passage in [23] to evaluate path smoothing approaches. For each scenario, several

<sup>2</sup>These simulation models are available at <https://github.com/NKU-MobFly-Robotics/local-planning-benchmark>.

TABLE II  
QUANTITATIVE STATISTICS OF PATH SMOOTHING RESULTS IN SIMULATION

		Travel Distance		Efficiency				Smoothness			
		$S$ [m]		$T$ [s]		$C$ [ms]		$K_{max}$		$K_{mean}$	
		<i>SBA</i>	<i>Ours</i>	<i>SBA</i>	<i>Ours</i>	<i>SBA</i>	<i>Ours</i>	<i>SBA</i>	<i>Ours</i>	<i>SBA</i>	<i>Ours</i>
Shopping Mall	1	29.28	<b>28.92</b>	73.23	<b>71.98</b>	3.19	<b>0.50</b>	1.90	<b>1.54</b>	0.33	<b>0.32</b>
	2	25.43	<b>25.05</b>	64.18	<b>62.78</b>	2.86	<b>0.50</b>	2.68	<b>2.13</b>	0.37	<b>0.34</b>
	3	58.52	<b>57.84</b>	141.39	<b>136.64</b>	2.65	<b>0.48</b>	1.76	<b>1.33</b>	0.24	<b>0.22</b>
Complex Maze	1	41.88	<b>40.52</b>	93.85	<b>91.44</b>	6.58	<b>0.66</b>	2.02	2.25	0.47	<b>0.46</b>
	2	53.45	<b>51.47</b>	121.24	<b>116.99</b>	10.21	<b>0.61</b>	2.86	<b>2.20</b>	<b>0.58</b>	0.59
	3	54.50	<b>52.61</b>	123.28	<b>119.74</b>	7.48	<b>0.61</b>	2.13	<b>2.08</b>	0.52	<b>0.49</b>
Narrow Passage	1	26.20	<b>25.76</b>	54.47	<b>54.21</b>	11.51	<b>0.62</b>	2.64	<b>1.92</b>	0.56	<b>0.53</b>
	2	30.07	<b>29.45</b>	62.59	<b>62.07</b>	13.19	<b>0.67</b>	1.84	1.84	0.65	<b>0.63</b>

sets of different start and goal configurations are selected for testing. Table II presents some quantitative statistics of simulation results.

As shown in Table II, the travel distance of the proposed approach is reduced by an average of 0.96 m. Accordingly, the motion efficiency of the proposed path smoothing approach is improved. Furthermore, because the proposed approach models the path smoothing problem as a convex QP problem, while the optimization objective of SBA contains both convex and non-convex terms, the computational efficiency of the proposed approach has been significantly improved. As shown in Table II, the consumed times of the proposed approach are all less than 0.7 ms, and smoothing path with the proposed approach is averagely 11.86 times faster than smoothing path with SBA. Especially in the complex maze and narrow passage scenarios, the computational efficiency of the proposed approach is 12.99 and 19.13 times faster than that of SBA, respectively. In addition, the smoothness of motion guidance provided by the proposed approach is commensurate with SBA.

## VI. EXPERIMENTS

In this section, outdoor experimental results in our campus are presented to validate the effectiveness of  $G^2VD$  planner.

### A. Experimental Setup

As shown in Fig. 1, the mobile robot SUMMIT-XL HL is used as the experimental platform, which is equipped with a Velodyne VLP-16 LiDAR, an Intel Realsense D435i depth camera, and an Intel NUC computer. The maximum linear acceleration of the robot is  $1.0 \text{ m/s}^2$ . Considering the safety of robot navigation, the maximum linear velocity is set to  $1.5 \text{ m/s}$  in the experiments.

To generate a prior global map for autonomous navigation, we first employ a LiDAR-inertial odometry algorithm described in [24] to build a large-scale 3-D point cloud map. And then, a point clouds segmentation algorithm presented in [25] is used to filter out point clouds that hit the ground and tree canopy. Finally, the filtered point clouds are projected

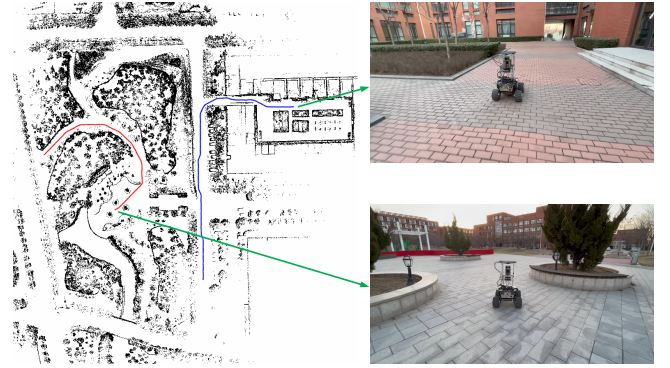


Fig. 7. Occupancy grid map for outdoor navigation. The dimension of the environment is approximately  $210 \times 220 \text{ m}^2$ . The routes of two sets of robot navigation are colored in red and blue, respectively.

to a 2-D plane to derive traversable regions in the form of occupancy grid map, as shown in Fig. 7. The dimension of the environment is approximately  $210 \times 220 \text{ m}^2$ . During robot navigation, the LiDAR-inertial odometry algorithm [24] and the point clouds segmentation algorithm [25] are also utilized to provide state estimation and local traversable regions for the robot, respectively.

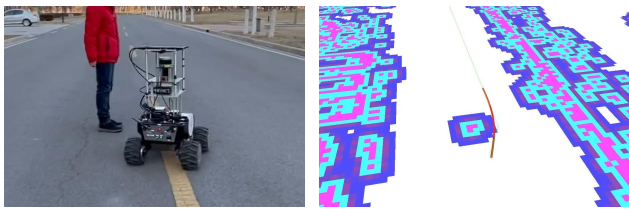
### B. Autonomous Navigation

As illustrated in Fig. 7, we select two sets of different start and goal configurations for outdoor navigation. The total travel distances of these two sets of outdoor navigation are approximately 118.3 m and 165.9 m, respectively.

Here we summarize several representative experimental results of autonomous navigation to demonstrate the key characteristics of  $G^2VD$  planner. More details are included in the video.

1) *Dealing With Static Obstacles*: Fig. 8(a) illustrates the scenario with static obstacles. The robot avoids a stationary person smoothly, according to the reliable path smoothing results.

2) *Dealing With Dynamic Obstacles*: Fig. 8(b) shows the scenario with dynamic obstacles. The robot implements fast



(a) Dealing with static obstacles.



(b) Dealing with dynamic obstacles.

Fig. 8. Screenshots of outdoor navigation results. The green curve denotes the path generated by the state lattice-based path planner, and the red curve represents the path smoothed by the proposed path smoothing approach.

re-planning and avoids an oncoming person successfully, thanks to the efficient path smoothing approach.

## VII. CONCLUSION

In this letter, an efficient motion planning approach called  $G^2VD$  planner is newly proposed for mobile robots. Based on a grid-based GVD, a novel Voronoi corridor is proposed and fully integrated into the state lattice-based path planner to further improve the search efficiency, along with a Voronoi potential field constructed to make the searched path keep a reasonable distance from obstacles to provide sufficient optimization margin for further path smoothing. And an efficient QP-based path smoothing approach is presented, wherein the clearance to obstacles is considered in the form of the penalty of the deviation from the safe reference path to improve the path clearance of hard-constrained path smoothing approaches. The performance of  $G^2VD$  planner is validated in various complex simulation scenarios and large-scale outdoor environments.

## REFERENCES

- [1] L. Palmieri, L. Bruns, M. Meurer, and K. O. Arras, "Dispartio: Optimal sampling for safe deterministic motion planning," *IEEE Robotics and Automation Letters*, vol. 5, no. 2, pp. 362–368, 2019.
- [2] J. Li, M. Ran, and L. Xie, "Efficient trajectory planning for multiple non-holonomic mobile robots via prioritized trajectory optimization," *IEEE Robotics and Automation Letters*, vol. 6, no. 2, pp. 405–412, 2020.
- [3] D. Le and E. Plaku, "Multi-robot motion planning with dynamics via coordinated sampling-based expansion guided by multi-agent search," *IEEE Robotics and Automation Letters*, vol. 4, no. 2, pp. 1868–1875, 2019.
- [4] L. E. Kavraki, P. Svestka, J.-C. Latombe, and M. H. Overmars, "Probabilistic roadmaps for path planning in high-dimensional configuration spaces," *IEEE Transactions on Robotics and Automation*, vol. 12, no. 4, pp. 566–580, 1996.
- [5] S. M. LaValle and J. J. Kuffner, "Randomized kinodynamic planning," *The International Journal of Robotics Research*, vol. 20, no. 5, pp. 378–400, 2001.
- [6] S. Karaman and E. Frazzoli, "Sampling-based algorithms for optimal motion planning," *The International Journal of Robotics Research*, vol. 30, no. 7, pp. 846–894, 2011.

- [7] P. E. Hart, N. J. Nilsson, and B. Raphael, "A formal basis for the heuristic determination of minimum cost paths," *IEEE Transactions on Systems Science and Cybernetics*, vol. 4, no. 2, pp. 100–107, 1968.
- [8] A. Ravankar, A. A. Ravankar, Y. Kobayashi, Y. Hoshino, and C.-C. Peng, "Path smoothing techniques in robot navigation: State-of-the-art, current and future challenges," *Sensors*, vol. 18, no. 9, pp. 1–30, 2018.
- [9] M. Likhachev and D. Ferguson, "Planning long dynamically feasible maneuvers for autonomous vehicles," *The International Journal of Robotics Research*, vol. 28, no. 8, pp. 933–945, 2009.
- [10] M. Pivtoraiko, R. A. Knepper, and A. Kelly, "Differentially constrained mobile robot motion planning in state lattices," *Journal of Field Robotics*, vol. 26, no. 3, pp. 308–333, 2009.
- [11] D. Ferguson, T. M. Howard, and M. Likhachev, "Motion planning in urban environments," *Journal of Field Robotics*, vol. 25, no. 11–12, pp. 939–960, 2008.
- [12] H. Choset and J. Burdick, "Sensor-based exploration: The hierarchical generalized Voronoi graph," *The International Journal of Robotics Research*, vol. 19, no. 2, pp. 96–125, 2000.
- [13] J. Ziegler, M. Werling, and J. Schroder, "Navigating car-like robots in unstructured environments using an obstacle sensitive cost function," in *Proceedings of the 2008 IEEE Intelligent Vehicles Symposium*, 2008, pp. 787–791.
- [14] D. Dolgov, S. Thrun, M. Montemerlo, and J. Diebel, "Path planning for autonomous vehicles in unknown semi-structured environments," *The International Journal of Robotics Research*, vol. 29, no. 5, pp. 485–501, 2010.
- [15] J. Wen, X. Zhang, H. Gao, J. Yuan, and Y. Fang, "E<sup>3</sup>MoP: Efficient motion planning based on heuristic-guided motion primitives pruning and path optimization with sparse-banded structure," *IEEE Transactions on Automation Science and Engineering*, 2021, doi: 10.1109/TASE.2021.3128521.
- [16] J. Zhou, R. He, Y. Wang, S. Jiang, Z. Zhu, J. Hu, J. Miao, and Q. Luo, "Autonomous driving trajectory optimization with dual-loop iterative anchoring path smoothing and piecewise-jerk speed optimization," *IEEE Robotics and Automation Letters*, vol. 6, no. 2, pp. 439–446, 2021.
- [17] P. Shen, X. Zhang, and Y. Fang, "Essential properties of numerical integration for time-optimal path-constrained trajectory planning," *IEEE Robotics and Automation Letters*, vol. 2, no. 2, pp. 888–895, 2017.
- [18] B. Lau, C. Sprunk, and W. Burgard, "Efficient grid-based spatial representations for robot navigation in dynamic environments," *Robotics and Autonomous Systems*, vol. 61, no. 10, pp. 1116–1130, 2013.
- [19] X. Zhang, J. Wang, Y. Fang, and J. Yuan, "Multilevel humanlike motion planning for mobile robots in complex indoor environments," *IEEE Transactions on Automation Science and Engineering*, vol. 16, no. 3, pp. 1244–1258, 2019.
- [20] P. F. Felzenszwalb and D. P. Huttenlocher, "Distance transforms of sampled functions," *Theory of Computing*, vol. 8, no. 1, pp. 415–428, 2012.
- [21] B. Stellato, G. Banjac, P. Goulart, A. Bemporad, and S. Boyd, "OSQP: An operator splitting solver for quadratic programs," *Mathematical Programming Computation*, vol. 12, no. 4, pp. 637–672, 2020.
- [22] N. Koenig and A. Howard, "Design and use paradigms for Gazebo, an open-source multi-robot simulator," in *Proceedings of the 2004 IEEE/RSJ International Conference on Intelligent Robots and Systems*, 2004, pp. 2149–2154.
- [23] J. Wen, X. Zhang, Q. Bi, Z. Pan, Y. Feng, J. Yuan, and Y. Fang, "MRPB 1.0: A unified benchmark for the evaluation of mobile robot local planning approaches," in *Proceedings of the 2021 IEEE International Conference on Robotics and Automation*, 2021, pp. 8238–8244.
- [24] T. Shan, B. Englot, D. Meyers, W. Wang, C. Ratti, and R. Daniela, "LIO-SAM: Tightly-coupled lidar inertial odometry via smoothing and mapping," in *Proceedings of the 2020 IEEE/RSJ International Conference on Intelligent Robots and Systems*, 2020, pp. 5135–5142.
- [25] H. Liu, R. Song, X. Zhang, and H. Liu, "Point clouds segmentation based on Euclidean clustering and multi-plane extraction in rugged field," *Measurement Science and Technology*, vol. 32, no. 9, pp. 1–14, 2021.